Performance evaluation of an integrated energy system for the production and use of renewable methanol via water electrolysis and CO$_2$ hydrogenation

Francesco Lonis, Vittorio Tola, Mario Cascetta, et al.

View Online

Export Citation

ARTICLES YOU MAY BE INTERESTED IN

Performance evaluation of an integrated energy system for the production and use of renewable methanol via water electrolysis and CO₂ hydrogenation

Francesco Lonis[1, a)] Vittorio Tola[1, b)] Mario Cascetta[1, c)] Simone Arena[1, d)]
Giorgio Cau[1, e)]

[1]Department of Mechanical, Chemical and Materials Engineering, University of Cagliari, Via Marengo 2, 09123
Cagliari, Italy

[a)] francesco.lonis@unica.it
[b)] vittorio.tola@dimcm.unica.it
[c)] mario.cascetta@unica.it
[d)] simonearena@unica.it
[e)] gcau@unica.it

Abstract. Aiming at the decarbonization of society, power-to-liquids processes can favour the exploitation of the excess of renewable energy, producing methanol or other chemicals (such as dimethyl ether) by reacting electrolytic hydrogen and recycled CO₂ (captured from industrial and power plants or directly from air). Such a system could behave as:
- an energy storage system, storing excess renewable energy as chemical energy in liquid fuels and converting it into electricity during lack of renewable energy,
- a source of fuels and chemicals for a variety of applications in many industrial sectors.

This work concerns the conceptual design and performance analysis of a small-scale integrated energy system for the production and use of methanol from renewable hydrogen and captured CO₂. The main components of the system are:
- a reversible high temperature and high efficiency solid oxide cell (RSOC) that can operate in charge (electrolyser, SOEC) and discharge (fuel cell, SOFC) mode to store and use electricity using methanol as energy storage medium,
- a catalytic reactor for methanol synthesis via CO₂ hydrogenation.

A thermal energy storage (TES) system based on a phase change material (PCM) is also included.

To predict performance of the main components and of the overall system, numerical simulation models were developed. Performance and efficiencies of each system component and of the overall system were evaluated through extensive mass and energy balances, considering two different configurations with and without TES integration. Performance indexes were calculated to analyse the goodness of introducing a TES. The global efficiency of the overall system increases from 30% to 35% when heat is recovered between sections via the TES system.

NOMENCLATURE

CRI	Carbon Recycling International	PtX	Power-to-X
GWHX	Gas-water heat exchanger	RES	Renewable energy sources
LHTES	Latent heat thermal energy storage	RSOC	Reversible solid oxide cell
MeOH	Methanol	SOC	Solid oxide cell
MSS	Methanol synthesis section	SOEC	Solid oxide electrolyzer cell
PCM	Phase change material	SOFC	Solid oxide fuel cell
PtL	Power-to-liquids	TES	Thermal energy storage

INTRODUCTION

The reduction of CO_2 emissions to restrain climate change is of fundamental importance. Since it is impractical to eliminate the dependence on fossil fuels completely in the short term, it is mandatory the development of energy systems capable of reducing fossil fuels utilization and the impact of their emissions, allowing a smooth transition to a decarbonized society based on low-carbon technologies. Power-to-X (PtX) represents an interesting approach to this low-carbon transition, allowing the production of chemicals and synthetic fuels via renewable energy sources (RES) and captured CO_2. In such a process, the low carbon footprint of clean energy sources is coupled to the advantages of fossil fuels, i.e. high energy intensity, density, and reliability [1]. Ideally, a closed carbon cycle would allow the capture of the atmospheric CO_2 directly, stabilizing the overall CO_2 concentration in the atmosphere. Numerous studies on different PtX systems can be found in literature, as for example [2–5], and others have been published on the valorization of CO_2 via renewable hydrogen [6–10].

Power-to-methanol is addressed in this work since methanol (often shortened to MeOH) is considered as one of the most promising liquid chemicals within the power-to-liquids (PtL) field. Olah et al. [11] even theorized a future methanol economy as an alternative to the hydrogen economy, owing to methanol higher energy density, both by weight and volume [11]. Many sectors would benefit from renewable methanol since it can be widely used as a fuel for power generation systems (fuel cells and gas turbines), residential, and transportation (automotive, naval, and aerial) sectors. Methanol can also be used as an energy storage medium, and as a chemical feedstock in industry, being a precursor for chemical compounds that are typically derived from fossil fuels, such as formaldehyde, acetic acid, dimethyl ether, gasoline, diesel and others [12]. Finally, from the energy storage perspective, methanol production would help to boost RES penetration, usability, and dispatchability, increasing RES reliability [13].

Nowadays, the only existing renewable methanol commercial facility is the Carbon Recycling International (CRI) George Olah Plant, located in Iceland [14]. Methanol is produced via CO_2 hydrogenation at a rate of 4000 t/y using hydrogen from renewable alkaline water electrolysis and recycled CO_2, which is captured from a near geothermal plant [15]. This facility is significantly smaller than conventional medium-scale methanol production plants from fossil fuels, usually characterized by a methanol output of around 1500 t/d [16]. Methanol is blended with gasoline for automotive mobility in the Country. The plant is connected to the local grid which is completely powered by RES (hydroelectric, wind, and geothermal). It is also planned to deploy other commercial plants based on the CRI "Emissions-to-Liquids" technology across Europe within the EU Horizon 2020 Research Program [17].

In this study the focus is on the production and use of methanol through high temperature reversible solid oxide cells (RSOC). RSOCs can work both as electrolyzers or as fuel cells at temperature as high as 700-1000 °C [18], leading to a high efficiency in both modes. In the case of excess of electricity generation from RES, the RSOC produces hydrogen (charge mode), which feeds a subsequent methanol synthesis section (MSS), to be converted along with CO_2 into methanol via catalytic CO_2 hydrogenation. Then methanol is stored at ambient conditions. Subsequently, in the case of lack of electricity production, the methanol feeds the RSOC, operating as a fuel cell, to produce electricity to level out peak demand (discharge mode). During discharge mode, excess heat generated in the SOFC (solid oxide fuel cell) section is stored in a thermal energy storage (TES) system based on a phase change material (PCM). The heat stored is exploited to perform water vaporization in the SOEC (solid oxide electrolyzer cell) section during hydrogen production. Other thermal integrations within each section and between different sections were considered and analyzed to recover and reuse as much heat as possible, reducing the supply of external energy. Electrochemistry and kinetic models were developed and implemented in Aspen Plus to simulate the cell behavior (in both operating modes) and the CO_2 hydrogenation process. Each section was characterized by a performance index defined considering mass and energy balances. Finally, comprehensive efficiency chains were defined and evaluated considering the interactions between each subsystem.

SYSTEM CHARACTERIZATION AND MODELS DESCRIPTION

Overall Plant Configuration

The system for the production and use of renewable methanol studied in this paper is composed of three main sections: a) an RSOC section capable of working as a SOEC or as a SOFC, depending on RES availability, b) a methanol synthesis and purification section and c) a TES section to heat recovery. Figure 1 shows a simplified scheme of the overall system and the interconnections between sections. Water, air, and renewable electricity feed the SOEC to produce hydrogen, and air rich in oxygen as a by-product. Hydrogen and previously captured CO_2 (process not accounted in this study) are compressed to the operating pressure of the methanol reactor where

catalytic CO_2 hydrogenation takes place. Unreacted gases are recycled, and crude methanol is purified in a distillation column and stored at ambient conditions. Then during discharge mode, the methanol is reformed to hydrogen that is oxidized in the SOFC. The heat integration block appearing in the functional scheme of Fig. 1 represents the heat transfer processes required to allow the system to reach operating conditions. A detail of the heat recovery (TES) section is reported in the lower-right corner of Fig. 1. The magnification shows the TES, a gas-water heat exchanger (GWHX), and the interactions between the SOFC gases, the TES, the air, and the water. During charge mode, the SOFC gases heat up the TES. During discharge mode, air circulates in a closed loop gaining heat from the TES and releasing it inside the GWHX to the water feeding the SOEC.
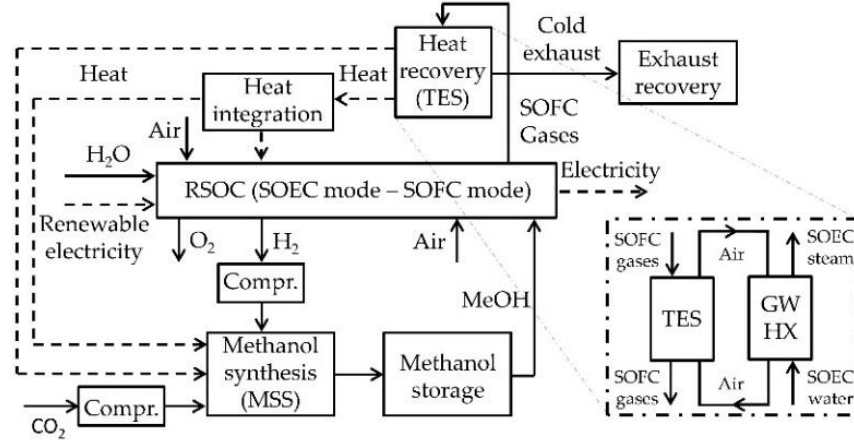

FIGURE 1 Simplified functional scheme of the overall system and detail of the heat recovery (TES) section

The overall system was sized to produce 1 MW of electrical energy in SOFC mode. Such a power requires a renewable methanol production of around 370 kg/h, in the order of the capacity of the only existing renewable methanol plant [14]. Flowrates of air, water and CO_2 feeding the SOEC and MSS sections were calculated for assuring such a methanol production.

Characterization and modeling of the main sections

Reversible Solid Oxide Cell Section

High temperature SOC are advantageous in both operating modes. In water electrolysis, both electricity and heat demand depend on the temperature. The higher the temperature, the lower the electricity and the higher the heat required, while the total energy demand slightly increases [19]. In fact, the increase of temperature reduces the overvoltages, especially the ohmic one, due to a better reactions kinetic. Similarly, in fuel cell operation, high temperature reduces the overvoltage losses, thus increasing the net power. Moreover, in both operating modes high temperature reactions require simple ceramic materials without expensive catalysts. In addition, ceramic materials are not subjected to carbon poisoning, typical of low temperature fuel cells. However, high temperature operation is responsible for significant mechanical and thermal stress, thus materials and assembly must be chosen and performed wisely. Since methanol production and use are differed during the day, coupling these two operating modes in one device allows saving investment costs and addressing different markets with the same system, such as energy storage, PtX, distributed power generation [6,20]. Switching from charge to discharge mode and vice versa requires only a few minutes [21].

SOEC technology has been receiving a growing attention in the last few years as a high efficiency device to produce hydrogen from water electrolysis. SOECs development stems from commercially existing SOFC, typically available in a range from 10 kW to 1 MW [22]. Since SOEC systems based on SOFC technology, and RSOC devices are relatively new technologies, state of the art modules produce only around 50 kW in SOFC mode and absorb around 150 kW in SOEC mode. However, in a future perspective, an RSOC based on the top end of the present SOFC size (1 MW) was considered in this work.

Even though they refer to two different operating modes of the same RSOC, the SOEC and SOFC sections were treated separately using dedicated models. Electrochemical and mathematical models based on equations proposed by Ni et al. [23–25] were implemented in Aspen Plus environment to simulate water splitting (and fuel oxidation) rigorously. The main phenomena occurring in a cell during electrolysis (or fuel oxidation during SOFC operation)

are described through special equations and theories: Nernst equation, reversible potential equation, Butler-Volmer equations, concentration overpotential theories, Bosanquet and Chapman-Enskog theories of gas diffusion. The same electrochemical model, slightly different in the concentration overpotential definition, was used in both SOEC and SOFC. Detailed and comprehensive description of the models and their parameters are found in Lonis et al. [26].

The SOEC analyzed in this paper requires to be fed by around 780 kg/h of water for producing the hydrogen flowrate feeding the MSS section. In the SOEC, water electrolysis is performed at ambient pressure and at 850 °C. At the selected operating conditions, thermo-neutral operation is performed, thus no external heat is required.

On the anode side, the cold sweep air is preheated (absorbing around 200 kW) from ambient conditions to 800°C, exploiting the thermal energy of the hot anode air (rich in oxygen) exiting the SOEC at 850 °C. Thus, an external heater provides further 15 kW to reach the final cell temperature. On the cathode side water is preheated, vaporized and superheated through two different sources to reach the operating temperature before entering the cell. A fraction of the water flowrate (about 185 out of the total 780 kg/h) is preheated and vaporized exploiting the residual heat of the hot anode exhaust. The remainder is preheated and vaporized (425 kW) by an external source or harvesting the heat from the SOFC exhaust gases stored in the TES system during discharge mode. Then, saturated steam is superheated to around 680 °C exploiting the hot cathode exhaust (composed of hydrogen and water). An external heater is required to reach the SOEC operating temperature (850 °C), absorbing a power of around 85 kW. In addition, a portion of the cathode exhaust is recycled to the cell inlet to reach a suitable feed composition (90% water, 10% hydrogen) to avoid electrode oxidation [27].

Starting from a water flowrate of around 780 kg/h and assuming a water utilization factor of 0.85, the SOEC produces around 76 kg/h of H_2 with an electrical power requirement of around 2.6 MW. Table 1 summarizes the energy balance relative to the heating and cooling processes within the SOEC system.

TABLE 1. Main heat transfers in the SOEC

Heating process	Heat (kW)	Cooling process	Heat (kW)
Sweep air PH by heat recovery	197.8	Anode exhaust 1st cooling	-197.8
Sweep air PH by external source	13.8	Anode exhaust 2nd cooling	-133.9
Water PH and VAP by heat recovery	133.9	Cathode exhaust cooling	-260.8
Water PH and VAP by external source or TES	426.6		
Steam SH by heat recovery	260.8		
Steam SH by external source	84.5		
PH: preheating; VAP: vaporization; SH: superheating			

Methanol Synthesis Section

The MSS is mainly composed of an adiabatic catalytic reactor for producing methanol via CO_2 hydrogenation and a methanol purification column [28]. Methanol is produced according to the reverse water gas shift reaction (1), the CO hydrogenation reaction (2), and the CO_2 hydrogenation reaction (3).

$$CO_2 + H_2 \rightleftarrows CO + H_2O \tag{1}$$

$$CO + 2H_2 \rightleftarrows CH_3OH \tag{2}$$

$$CO_2 + 3H_2 \rightleftarrows CH_3OH + H_2O \tag{3}$$

The catalytic reaction over the commercial catalyst $Cu/ZnO/Al_2O_3$ was simulated by implementing a Langmuir-Hinshelwood Hougen-Watson (LHHW) kinetic model originally developed by Vanden Bussche and Froment [29] and adapted by Van-Dal and Bouallou [28]. The model was implemented within an RPlug reactor as comprehensively reported in Al-Malah [30].

By assuming the same duration of the charging and discharging process of 6 hours, the methanol flowrate produced in the MSS was set equal to that consumed in the SOFC (around 370 kg/h). By assuming a molar ratio equal to the stoichiometric one in reaction (3), such a methanol production requires a flowrate of H_2 and CO_2 equal to around 76 kg/h and 550 kg/h, respectively. The feeding flows (H_2 and CO_2) are compressed to the operating pressure (65 bar) through two trains of three intercooled compressors each. The total power absorbed by the compressors is around 240 kW. Then the reactants are preheated to 210 °C before entering the reactor. Since the global CO_2 hydrogenation process is exothermic and the reactor is supposed adiabatic, the temperature increases to around 290 °C. The reactor exhaust (mainly H_2, and only around 4% by volume of methanol, Table 2) is purified from unreacted species and incondensable gases, which are recycled back to the reactor inlet to boost methanol

production, via two flash processes. The first flash occurs at a temperature of 50 °C and a pressure of 65 bar. Then the pressure and temperature of the liquid stream are reduced to around 1.2 bar and 22 °C respectively, and the flow is subjected to the second flash process. The crude methanol exiting the second flash is sent to a distillation column, where the reboiling duty allows the separation of water and methanol. The distillate at the top of the column is a mixture of methanol and CO_2, with a methanol purity of around 95.1% (by weight). The unreacted CO_2 is separated from methanol by simply condensing the latter.

Table 2 shows the composition of the main streams of the methanol purification section.

TABLE 2. Main streams composition

Chemical species	Reactor exhaust (vol%)	Liquid from flash 1 (wt%)	Crude methanol (wt%)	Distillate (wt%)
CH_3OH	0.0384	0.4909	0.6167	0.9513
H_2	0.7728	0.0000	0.0000	0.0000
CO_2	0.1032	0.2310	0.0316	0.0487
CO	0.0486	0.0022	0.0000	0.0000
H_2O	0.0370	0.2759	0.3517	0.0000

To reduce the heat requirements in the MSS a heat integration was implemented inside it. The preheating of the reactants (around 350 kW) is carried out by exploiting the heat of the reactor exhaust, reducing its temperature from 290 to 175 °C. Since the reboiling process in the distillation column requires 180 kW at a constant temperature of 100 °C, heat is still provided by the same reactor exhaust, that cools down from 175 to 124 °C. Finally, the reactor exhaust heats the crude methanol up to the inlet temperature of the distillation column (80 °C), allowing a further recovery of around 135 kW. Globally, a total of around 665 kW is recovered within the MSS. Detailed and comprehensive description of the simulation models and their parameters are found in Lonis et al. [26].

Solid Oxide Fuel Cell Section

As previously specified, the SOFC was sized to produce a power of 1 MW. The SOFC section is fed with methanol, along with water and air. Methanol and water are vaporized and mixed together with a portion of the cell outlet to reach a temperature of 300 °C. Then, methanol is reformed to a hydrogen rich mixture (H_2 content about 64% by vol.) to produce electricity in the cell. Water flowrate is obtained setting a desired steam to carbon ratio in the reformer. As the SOEC, the SOFC operates at a temperature of 850 °C with a fuel utilization factor of 0.85. Residual gases from SOFC, mainly composed of H_2 and CO, are burnt in a post combustor increasing the exhaust temperature. The exhaust gases are used to preheat the inlet air, and thus are cooled down to 380 °C. Finally, the residual heat can be stored in a TES system to provide energy for water preheating and vaporization in the SOEC during charge mode, substituting the external heater.

Thermal Energy Storage Section

A latent heat thermal energy storage system (LHTES) was analyzed in this paper and NaOH was identified as a suitable PCM for the considered application. Table 3 reports the main characteristics of the PCM chosen [31].

TABLE 3. Main characteristics of the PCM

Characteristic	Value
Phase change temperature [°C]	318
Latent heat of fusion [kJ/kg]	165
Mean density [kg/m^3]	2100
Specific heat [J/(kgK)]	2080

A preliminary design of the LHTES system was carried out using a numerical simulation model specifically developed in the Matlab-Simulink environment based on a transient one-dimensional (1-D) two-equation model (LTNE). This model allows analyzing the behavior of the storage unit and finding the optimal size configuration by calculating the temperature behavior of the heat thermal fluid and the PCM. The TES system consists of a single-tank based on a packed bed configuration using PCM held in capsules 0.05 m in diameter. The porous bed is considered homogeneous and isotropic, the energy losses are supposed negligible, while the shape of the

thermocline generated within the bed along the axis of the tank is calculated by considering the radial temperature profile constant. A detailed description of the model adopted is reported in previous works [32,33], where the apparent heat capacity method was used to model the PCM melting process.

A simplified scheme of the PCM-TES plus the GWHX is reported in Fig. 1. During the charge phase, hot gases at 380 °C provided by the SOFC enter from the top of the unit, releasing thermal energy to the PCM, and exit from the bottom. During the discharge phase, the direction of the flow is reversed, and an air flow enters from the bottom recovering the heat from the PCM. Then the hot air enters in a GWHX preheating and vaporizing the water feeding the SOEC. Globally, a total thermal energy of around 2.5 MWh is exchanged within the TES system and the GWHX during the 6-hour operation.

Performances Indexes

To evaluate the performance of the proposed energy system, performance indexes of each section and of the overall system were defined. The definition of a global performance index is not straightforward owing to the level of complexity and the coexistence of different forms of energy entering and exiting the subsystems. Performance indexes of the various subsystems were defined and linked together in order to attain an overall performance index, as reported in a previous work by the same authors [26].

The efficiency of the water electrolysis η_{SOEC} is defined by Eq. (4), where $\dot{m}_{H_2} \cdot H_{i,H_2}$ is the hydrogen chemical power ($\dot{m}_{H_2}$ hydrogen mass flow; H_{i,H_2} lower heating value), P_{SOEC} and $P_{BOP,SOEC}$ are the electric power of the SOEC and of its auxiliaries, respectively.

$$\eta_{SOEC} = \frac{\dot{m}_{H_2} \cdot H_{i,H_2}}{P_{SOEC} + P_{BOP,SOEC}} \tag{4}$$

The efficiency of the SOFC η_{SOFC} (Eq. (5)) is defined as the ratio between the net power output (P_{SOFC} electric power of the SOFC; $P_{BOP,SOFC}$ SOFC auxiliaries) and the methanol chemical power ($\dot{m}_{MeOH}$ methanol mass flow; $H_{i,MeOH}$ lower heating value) entering the SOFC.

$$\eta_{SOFC} = \frac{P_{SOFC} - P_{BOP,SOFC}}{\dot{m}_{MeOH} \cdot H_{i,MeOH}} \tag{5}$$

Both a gross ($\eta_{RSOC,G}$) and a net (η_{RSOC}) round trip efficiency can be defined, neglecting or considering the parasitic absorption of the auxiliaries as reported by Eq. (6) and (7), respectively:

$$\eta_{RSOC,G} = \frac{P_{SOFC}}{P_{SOEC}} \tag{6}$$

$$\eta_{RSOC} = \frac{P_{SOFC} - P_{BOP,SOFC}}{P_{SOEC} + P_{BOP,SOEC}} \tag{7}$$

Combining Eq. (4), (5) and (7), Eq. (8) is obtained. The term $\eta_{MSS,C}$ is expressed as the chemical conversion efficiency of the MSS, which is similar to a cold gas gasifier efficiency.

$$\eta_{RSOC} = \eta_{SOEC} \cdot \eta_{SOFC} \frac{\dot{m}_{MeOH} \cdot H_{i,MeOH}}{\dot{m}_{H_2} \cdot H_{i,H_2}} = \eta_{SOEC} \cdot \eta_{SOFC} \cdot \eta_{MSS,C} \tag{8}$$

The actual MSS efficiency η_{MSS}, Eq. (9), takes into account also the external power required in the reboiling process ($\dot{E}_{MSS}$) and the balance of plant absorption ($P_{BOP,MSS}$).

$$\eta_{MSS} = \frac{\dot{m}_{MeOH} \cdot H_{i,MeOH}}{\dot{m}_{H_2} \cdot H_{i,H_2} + \dot{E}_{MSS} + P_{BOP,MSS}} \tag{9}$$

The overall system is characterized by a global efficiency η_G defined by Eq. (10):

$$\eta_G = \frac{P_{SOFC} - P_{BOP,SOFC}}{P_{SOEC} + P_{BOP,SOEC} + \dot{E}_{MSS} + P_{BOP,MSS}} \tag{10}$$

By combining equation (10) with Eq. (4), (5) and (8), the global efficiency η_G can be expressed according to Eq. (11).

$$\eta_G = \eta_{SOEC} \cdot \eta_{SOFC} \cdot \eta_{MSS,C} \cdot \varphi_{SOEC} = \eta_{RSOC} \cdot \varphi_{SOEC} \tag{11}$$

where φ_{SOEC} is defined as the ratio between the power entering the electrolysis section and the total power entering the system as in Eq. (12).

$$\varphi_{SOEC} = \frac{P_{SOEC} + P_{BOP,SOEC}}{P_{SOEC} + P_{BOP,SOEC} + \dot{E}_{MSS} + P_{BOP,MSS}} \tag{12}$$

An alternative definition of the global efficiency can be found by combining Eq. (9) and (11):

$$\eta_G = \eta_{SOEC,R} \cdot \eta_{SOFC} \cdot \eta_{MSS} \tag{13}$$

where $\eta_{SOEC,R}$ (Eq. (14)) is a SOEC rectified efficiency, which would be equal to the SOEC efficiency when the MSS does not need external power supply.

$$\eta_{SOEC,R} = \frac{\dot{m}_{H_2} \cdot H_{i,H_2} + (\dot{E}_{MSS} + P_{BOP,MSS})}{P_{SOEC} + P_{BOP,SOEC} + (\dot{E}_{MSS} + P_{BOP,MSS})} \tag{14}$$

Consequently, an alternative expression of the RSOC efficiency is given by Eq. (15), obtained by combining Eq. (11) and (13).

$$\eta_{RSOC} = \frac{\eta_{SOEC,R}}{\varphi_{SOEC}} \cdot \eta_{SOFC} \cdot \eta_{MSS} \tag{15}$$

Finally, Eq. (16) synthetizes the correlation among the relevant parameters of the comprehensive SOEC-MSS system.

$$\eta_{SOEC} \cdot \varphi_{SOEC} \cdot \eta_{MSS,C} = \eta_{SOEC,R} \cdot \eta_{MSS} \tag{16}$$

In addition, a PtL efficiency η_{PtL} can be defined when SOEC and MSS are considered as a whole (Eq. (17)).

$$\eta_{PtL} = \frac{\dot{m}_{MeOH} \cdot H_{i,MeOH}}{P_{SOEC} + P_{BOP,SOEC} + \dot{E}_{MSS} + P_{BOP,MSS}} = \eta_{SOEC} \cdot \varphi_{SOEC} \cdot \eta_{MSS,C} \tag{17}$$

RESULTS AND DISCUSSION

Evolution of the TES Temperature Profiles

The temperature (thermocline) evolution of the TES system during the charging and discharging are shown in Fig. 2a and 2b for a period 6-hour long. The two figures represent regime conditions obtained after a transition period to warm-up the system. The TES system is sized for releasing the thermal power required by the SOEC during the system charge mode (around 425 kW), allowing the bed to store around 2.5 MWh for the 6-hour operation. Assuming a bed porosity of 0.4 and an aspect ratio of 1, both a bed diameter and height equal to 3 m were calculated. The TES system is considered adiabatic, thus the heat losses are neglected.
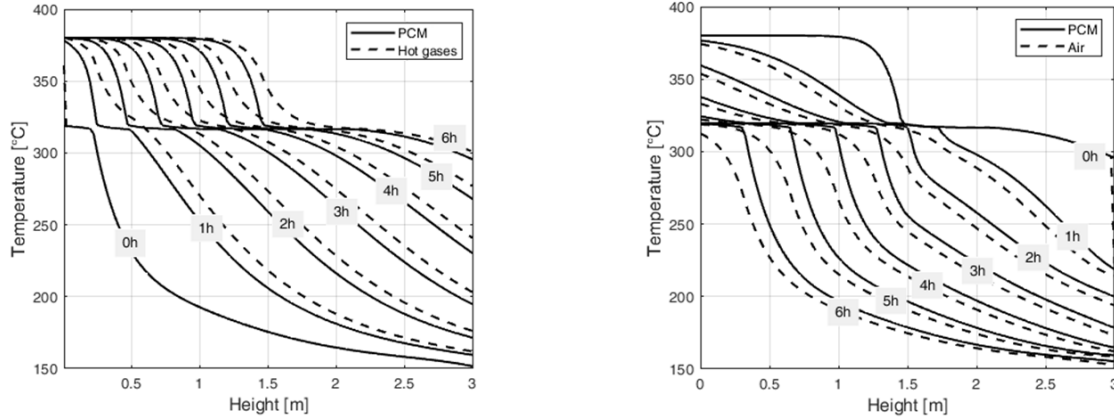

FIGURE 2 Thermocline evolution during the charge (a, left) and discharge phases (b, right)

In Fig. 2a and 2b, solid lines represent the temperature evolution of the PCM, while dotted lines represent the evolution of the hot gases (Fig. 2a) or cold air (Fig. 2b). During the charge phase (Fig. 2a) hot gases flow from the top to the bottom of the bed. Since Fig. 2a and 2b represent regime conditions, the temperature profile inside the bed at the beginning of the charge phase (0h) overlaps the temperature profile at the end of the previous discharge phase. Initially, the heat exchange takes place in form of sensible heat between the hot gases and the PCM in solid phase. Then, at around 320 °C the transition process occurs, and the heat is stored as latent. Finally, the heat transfer takes place again in form of sensible heat between the hot gases and the PCM in liquid phase. At the end of the charge phase (6h), around half of the PCM is in the liquid phase, while the remaining part is in transition or solid phase.

Figure 2b shows the discharging process during which air (2.4 kg/s) circulates in a closed-circuit recovering the heat stored in the PCM and releasing it to the water feeding the SOEC. In the discharge phase, the flow direction is reversed, thus the air flows from the bottom to the top of the tank. The beginning of the discharge phase (0h) coincides with the ending of the charge phase. As Fig. 2b shows, at the end of the discharge phase almost 80% of the thermal energy stored by the PCM bed is released, mainly in form of latent heat. Indeed, at the end of the discharging process only the upper layers of the bed are in liquid phase.

With the chosen TES configuration and size, the thermal power released by the TES system allows preheating and vaporizing the desired rate of water feeding the SOEC (0.17 kg/s).

Performance Indexes

Table 4 reports the data used to calculate the performance indexes of the system previously defined. The system was analyzed with (case A) and without (case B) the presence of the TES device to recover heat.

TABLE 4. Main results of the SOEC, MSS, and SOFC sections

Section	Process	Case	Power [kW]
SOEC	P_{SOEC}	A, B	2554
	$\dot{m}_{H_2} \cdot H_{i,H_2}$	A, B	2520
	$P_{BOP,SOEC}$	A	525
		B	98.3
Methanol synthesis	$\dot{m}_{MeOH} \cdot H_{i,MeOH}$	A, B	2033
	$\dot{m}_{H_2} \cdot H_{i,H_2}$	A, B	2520
	$P_{BOP,MSS}$	A, B	239
	$\dot{E}_{MSS}$	A, B	0
SOFC	P_{SOFC}	A, B	1000
	$\dot{m}_{MeOH} \cdot H_{i,MeOH}$	A, B	2033
	$P_{BOP,SOFC}$	A, B	0

As previously specified, the introduction of the TES allows saving around 425 kW in the SOEC, substituting the external heat supply for water vaporization. Since the reboiling heat ($\dot{E}_{MSS}$) is recovered from the hot exhaust of the reactor, the value reported in Table 4 is equal to 0. Similarly, since the SOFC auxiliaries absorb a negligible power, $P_{BOP,SOFC}$ is set equal to 0.

Table 5 shows the performance indexes calculated for both case A and case B. While in both cases the integration within each section was performed by recirculating outlet streams to preheat inlet streams, water vaporization heat was recovered via the TES system only in case B. Thus, case A is characterized by lower efficiencies due to higher energy requirements to be provided from the outside.

TABLE 5. Performance indexes results

Efficiency	A	B	Efficiency	A	B	Efficiency	A	B
η_{SOEC}	0.818	0.950	$\eta_{MSS,C}$	0.807	0.807	η_{SOFC}	0.492	0.492
$\eta_{SOEC,R}$	0.832	0.954	η_{MSS}	0.737	0.737	η_{RSOC}	0.325	0.377
φ_{SOEC}	0.928	0.917	η_{PtL}	0.613	0.703	η_G	0.300	0.346

The efficiency of the SOEC η_{SOEC} is considerably higher (around 0.82) than in conventional low temperature electrolyzers, since the process is carried out at high temperature reducing the electricity input. The thermal energy recovery by a TES system allows to further increase the SOEC efficiency up to 0.95. Since the methanol synthesis process is characterized by an efficiency η_{MSS} slightly lower than 0.75 for both cases, the PtL efficiency η_{PtL} is equal to 0.61 and 0.70 for case A and case B, respectively. Both SOEC and PtL efficiency values are consistent with literature data. The SOFC shows an efficiency η_{SOFC} slightly lower than 0.50, also consistent with literature values, mainly related to methanol conversion in the reformer. Globally, the efficiency of the RSOC is as low as 0.33-0.38. Finally, the base case, without TES system, leads to an efficiency of the overall system η_G equal to 0.30. The integration with the TES allows a better recovery of the heat released by the SOFC, boosting the global efficiency to 0.35.

Due to the presence of the SOFC that allows the storage of excess heat during the discharge mode, such a system can be operated as a standalone plant capable of behaving as an energy storage system and as a fuels and chemicals production facility.

CONCLUSIONS

Power-to-X technologies powered by renewable energy and fed with captured CO_2 might be part of the solution to the climate change problem. This paper concerns the conceptual design and performance analysis of an integrated energy system for the production and use of methanol from renewable hydrogen and captured CO_2. Methanol is

treated as a renewable energy storage medium and a hydrogen carrier. The system is composed of an RSOC capable of operating in both SOEC and SOFC mode, depending on renewable energy source availability, a methanol synthesis section (MSS), and a TES system based on a PCM. Hydrogen is produced from RES through the RSOC in SOEC mode and feeds the MSS along with CO_2 to produce methanol. Methanol is stored and subsequently feeds the RSOC in SOFC mode to produce electricity during peak demand. Excess of process heat is recovered to increase the global efficiency of the system. Each section of the overall system was analyzed thoroughly via comprehensive mathematical and electrochemical models.

The overall system was sized by imposing a SOFC power of around 1 MW, which requires the production of around 370 kg/h of methanol in the MSS. The RSOC absorbs around 2.5 MW when operating in SOEC mode. Performance of the overall system was calculated considering two different configurations: without and with TES integration. Without TES integration, the system shows a global efficiency of around 30%, while the thermal integration among sections with the introduction of a TES system boosts the global efficiency to around 35%. Indeed, the integration with the TES system reduces the thermal energy requirement inside the SOEC, allowing a thermal energy saving of around 425 kW.

A preliminary design of the TES system was carried out along with the dynamic analysis of the charging and discharging processes, resulting in a bed of encapsulated PCM of 3 meters in diameter and height.

Efficiency-wise, the results obtained are consistent with those reported in literature. Thus, the system proves to be a good way to store excess electricity in a stable and high energy density fuel. However, given the present high costs related to solid oxide technology, it is too early to expect a quick deployment of these technologies. If a totally favorable scenario is considered with stack lifespan improvement and electrolyzer cost reduction, methanol production via SOEC or RSOC will reach international market values in the near future, resulting in an interesting way of storing electricity and producing renewable fuels.

ACKNOWLEDGMENTS

REFERENCES

1   Ganesh I. Conversion of carbon dioxide into methanol - A potential liquid fuel: Fundamental challenges and opportunities (a review). Renew Sustain Energy Rev 2014;31:221–57. doi:10.1016/j.rser.2013.11.045.

2   O'Brien JE, McKellar MG, Stoots CM, Herring JS, Hawkes GL. Parametric study of large-scale production of syngas via high-temperature co-electrolysis. Int J Hydrogen Energy 2009;34:4216–26. doi:10.1016/j.ijhydene.2008.12.021.

3   Albrecht FG, Konig DH, Dietrich RU. The potential of using power-to-liquid plants for power storage purposes. Int Conf Eur Energy Mark EEM 2016;2016-July. doi:10.1109/EEM.2016.7521203.

4   Fasihi M, Bogdanov D, Breyer C. Techno-Economic Assessment of Power-to-Liquids (PtL) Fuels Production and Global Trading Based on Hybrid PV-Wind Power Plants. Energy Procedia 2016;99:243–68. doi:10.1016/j.egypro.2016.10.115.

5   Schmidt P, Batteiger V, Roth A, Weindorf W. Power-to-Liquids as Renewable Fuel Option for Aviation : A Review 2018:127–40. doi:10.1002/cite.201700129.

6   Mermelstein J, Posdziech O. Development and Demonstration of a Novel Reversible SOFC System for Utility and Micro Grid Energy Storage. Fuel Cells 2017;17:562–70. doi:10.1002/fuce.201600185.

7   Di Giorgio P, Desideri U. Potential of reversible solid oxide cells as electricity storage system. Energies 2016;9. doi:10.3390/en9080662.

8   Santhanam S, Heddrich MP, Riedel M, Friedrich KA. Theoretical and experimental study of Reversible Solid Oxide Cell (r-SOC) systems for energy storage. Energy 2017;141:202–14. doi:10.1016/j.energy.2017.09.081.

9   Mottaghizadeh P, Santhanam S, Heddrich MP, Friedrich KA, Rinaldi F. Process modeling of a reversible solid oxide cell (r-SOC) energy storage system utilizing commercially available SOC reactor. Energy Convers Manag 2017;142:477–93. doi:10.1016/j.enconman.2017.03.010.

10 Matzen M, Demirel Y. Methanol and dimethyl ether from renewable hydrogen and carbon dioxide: Alternative

fuels production and life-cycle assessment. J Clean Prod 2016;139:1068–77. doi:10.1016/j.jclepro.2016.08.163.

11 Olah GA, Goeppert A, Prakash GKS. Beyond Oil and Gas: The Methanol Economy. 2nd ed. Weinheim, Germany: Wiley-VCH Verlag GmbH & Co. KGaA; 2009. doi:10.1002/9783527627806.

12 Bertau M, Offermanns H, Plass L, Schmidt F. Methanol: The Basic Chemical and Energy Feedstock of the Future. 2014. doi:10.1007/978-3-642-39709-7.

13 Bergins C, Tran K, Koytsoumpa E, Kakaras E, Buddenberg T, Sigurbjörnsson Ó. Power to Methanol Solutions for Flexible and Sustainable Operations in Power and Process Industries. Power-Gen Eur 2015.

14 George Olah Plant — CRI - Carbon Recycling International n.d. http://carbonrecycling.is/george-olah/ (accessed July 19, 2018).

15 Atsonios K, Panopoulos KD, Kakaras E. Investigation of technical and economic aspects for methanol production through CO2 hydrogenation. Int J Hydrogen Energy 2016;41:2202–14. doi:10.1016/j.ijhydene.2015.12.074.

16 Al-Kalbani H, Xuan J, García S, Wang H. Comparative energetic assessment of methanol production from CO2: Chemical versus electrochemical process. Appl Energy 2016;165:1–13. doi:10.1016/j.apenergy.2015.12.027.

17 CRI awarded EU grant to scale ETL technology — CRI - Carbon Recycling International n.d. http://www.carbonrecycling.is/news/2019/4/10/cri-awarded-eu-grant-to-scale-etl-technology (accessed May 7, 2019).

18 Ni M, Zhao TS, editors. Solid Oxide Fuel Cells: From Materials to System Modeling. Cambridge: The Royal Society of Chemistry; 2013. doi:10.1039/9781849737777.

19 Ni M, Leung MKH, Leung DYC. Technological development of hydrogen production by solid oxide electrolyzer cell (SOEC). Int J Hydrogen Energy 2008;33:2337–54. doi:10.1016/j.ijhydene.2008.02.048.

20 Guan J, Minh N, Ramamurthi B, Ruud J, Hong J-K, Riley P, et al. High performance flexible reversible solid oxide fuel cell 2006.

21 Februar I. sunfire supplies Boeing with largest reversible solid oxide electrolyser/fuel cell system. Fuel Cells Bull 2016;2016:1. doi:10.1016/s1464-2859(16)70002-2.

22 Minh NQ. Solid oxide fuel cells for power generation and hydrogen production. J Korean Ceram Soc 2010;47:1–7. doi:10.4191/KCERS.2010.47.1.001.

23 Ni M, Leung MKH, Leung DYC. An electrochemical model of a solid oxide steam electrolyzer for hydrogen production. Chem Eng Technol 2006;29:636–42. doi:10.1002/ceat.200500378.

24 Ni M, Leung MKH, Leung DYC. Parametric study of solid oxide steam electrolyzer for hydrogen production. Int J Hydrogen Energy 2007;32:2305–13. doi:10.1016/j.ijhydene.2007.03.001.

25 Ni M, Leung MKH, Leung DYC. Parametric study of solid oxide fuel cell performance. Energy Convers Manag 2007;48:1525–35. doi:10.1016/j.enconman.2006.11.016.

26 Lonis F, Tola V, Cau G. Renewable methanol production and use through reversible solid oxide cells and recycled CO2 hydrogenation. Fuel 2019;246:500–15. doi:10.1016/j.fuel.2019.02.108.

27 Barelli L, Bidini G, Cinti G. Airflow Management in Solid Oxide Electrolyzer (SOE) Operation: Performance Analysis. ChemEngineering 2017;1:13. doi:10.3390/chemengineering1020013.

28 Van-Dal ÉS, Bouallou C. Design and simulation of a methanol production plant from CO2 hydrogenation. J Clean Prod 2013;57:38–45. doi:10.1016/j.jclepro.2013.06.008.

29 Bussche KM Vanden, Froment GFF. A Steady-State Kinetic Model for Methanol Synthesis and the Water Gas Shift Reaction on a Commercial Cu/ZnO/Al2O3Catalyst. J Catal 1996;161:1–10. doi:10.1006/jcat.1996.0156.

30 Al-Malah KIM. Aspen Plus®. Hoboken, NJ, USA: John Wiley & Sons, Inc.; 2016. doi:10.1002/9781119293644.

31 Agyenim F, Hewitt N, Eames P, Smyth M. A review of materials, heat transfer and phase change problem formulation for latent heat thermal energy storage systems (LHTESS). Renew Sustain Energy Rev 2010;14:615–28. doi:10.1016/j.rser.2009.10.015.

32 Cascetta M, Cau G, Puddu P, Serra F. Experimental investigation of a packed bed thermal energy. J Phys Conf Ser 2015;012018. doi:10.1088/1742-6596/655/1/012018.

33 Cascetta M, Serra F, Arena S, Casti E, Cau G, Puddu P. Experimental and Numerical Research Activity on a Packed Bed TES System. Energies 2016;9:1–13. doi:10.3390/en9090758.